Pei Lu, Yi Xing, Caiting Li, Renpeng Qing, Wei Su, Nian Liu

A reusable material with high performance for removing NO at room temperature: performance, mechanism and kinetics

Erstveröffentlichung in / First published in:
Catalysis Science & Technology. 2016, 6(10), S. 3520–3528 [Zugriff am: 01.11.2019]. Royal Society of Chemistry. ISSN 2044-4761.

DOI: https://doi.org/10.1039/c5cy01562f

Catalysis Science & Technology

PAPER

View Article Online
View Journal | View Issue

Cite this: *Catal. Sci. Technol.*, 2016, **6**, 3520

A reusable material with high performance for removing NO at room temperature: performance, mechanism and kinetics

Pei Lu,[a] Yi Xing,*[a] Caiting Li,*[b] Renpeng Qing,†[b] Wei Su[a] and Nian Liu[c]

Received 15th September 2015,
Accepted 8th December 2015

DOI: 10.1039/c5cy01562f

www.rsc.org/catalysis

Removing NO from the air with a reusable material at room temperature is challenging. In this study, a series of urea–MnO_x/ACF and urea–$x(CeO_2$–$(1-x)MnO_2)$/ACF materials were prepared and used for removing NO at room temperature. The results showed that 10% urea–8% ($0.5CeO_2$–$0.5MnO_2$)/ACF yielded the highest NO conversion, which showed an NO conversion ratio above 90% with 1000 ppm NO in the initial mixed gases. Moreover, the NO conversion exceeded 98% when the NO concentration was 100 ppm in the initial mixed gases. More importantly, 10% urea–8% ($0.5CeO_2$–$0.5MnO_2$)/ACF was stable even after it was regenerated by reloading with urea, demonstrating that the material could be easily reused and its high performance was maintained. Finally, the mechanism and kinetics of the NO removal was discussed.

1. Introduction

NO_x pollution seriously affects people's health, especially in developing countries. Much attention has been paid to removing NO_x from flue gas and many promising solutions have been reported.[1,2] Selective catalytic reduction (SCR) of NO with NH_3 has been the method most widely used by researchers over past decades owing to its high efficiency.[1,3,4] A series of catalysts, including noble metals,[5–7] transition metal oxides,[8–12] rare earth oxides,[13–15] and metal-modified zeolites,[3,16,17] have been used to control NO emission. The catalytic activity of these catalysts is high, and a good NO removal rate could be achieved. However, the experimental temperatures for these catalysts are usually above 120 °C and they have been mainly used for the removal of NO_x in industrial flue gases at elevated temperatures.[13,18] For controlling NO pollution around traffic intersections and along highways at ambient temperatures, set as 30 °C in this study, current catalysts are not active enough to attain high NO conversion.

The transition metal oxide catalysts manganese oxides and ceria[1,9,11–13,19,20] are promising for NO control under ambient conditions. With the redox cycle between Mn^{4+} and Mn^{3+}, Mn-containing catalysts show high catalytic activity under ambient conditions by transferring electrons easily. Meanwhile, the reaction between CeO_2 and Ce_2O_3 releases oxygen, promoting the oxidation of NO to NO_2. In addition, when mixed with manganese oxide ceria increases the oxygen storage capacity of MnO_x and greatly improves oxygen migration speed for heterogeneous catalysis.[1,21–25] Therefore, the synergistic effect between the two metal oxides could greatly improve the catalytic efficiency of the SCR of NO.

NO pollution at room temperature can be controlled by three main methods: photocatalytic oxidation by TiO_2,[26,27] biological oxidation,[28] and adsorption by carbon materials.[29] Photocatalysts are too expensive for NO control and biological oxidation is not suitable for urban NO pollution caused by vehicle release. Physical adsorption by activated carbon materials combined with a catalytic reaction by metal oxides loaded on the carbon materials would be the most suitable method for urban NO control at room temperature.[30] Owing to its large specific surface area and special pore-diameter distribution, activated carbon fiber has been widely used in air purification.[2,31] Urea[32,33] is one of the most promising reducing reagents for SCR systems, because of its high reactivity with NO_x at low temperatures.

Urea supported on heterogeneous catalysts may be an effective material for reducing NO to N_2.[18,34–36] Based on our earlier work, we are searching for a reusable material with high performance for removing NO from air at room temperature. In this study, a series of 10% urea–MnO_x/ACF and 10% urea–$(xCeO_2$–$(1-x)MnO_2)$/ACF materials were prepared for NO purification at room temperature and their performance, mechanism and kinetics were studied.

[a] *School of Civil and Environmental Engineering, University of Science and Technology Beijing, Beijing, 100083, China. E-mail: cnlupei@163.com, xing_bkd@163.com*
[b] *College of Environmental Science and Engineering, Hunan University, Changsha 410082, China. E-mail: ctli@hnu.edu.cn*
[c] *Faculty of Environmental Sciences, Dresden University of Technology, Dresden, 01069, Germany*
† The author contributed equally to the first author.

2. Experimental

2.1. Sample preparation

The rayon-based ACF, used as catalyst carrier in this study, was supplied by Sutong Carbon Fiber Company. The ACF was washed in deionized water and then dried at 105 °C for 4 h in an oven (DHG-9023A, Shanghai Qin Mai Instrument Co., Ltd.). The ACF was put in clean hermetic bags for further use.

The catalysts were prepared by the equal-volume impregnation method. ACF was dipped in a series of $Mn(AC)_2$ solutions for 2 h, where the mass fractions of MnO_2 were 5, 8, 10, and 12 wt%. The samples were dried at 105 °C and pyrolyzed at 420 °C for 2 h in an N_2 stream. Subsequently, the catalysts were ground to a powder, and then dipped in 10 wt% urea solution for 24 h. The samples were dried at 50 °C in a vacuum oven to obtain the urea–MnO_x/ACF series samples.

CeO_2 and MnO_x at mass ratios of 1 : 3, 1 : 2, 1 : 1, 2 : 1, and 3 : 1 were deposited onto ACF through a similar co-impregnation method, and the material was then loaded with urea. A series of 10% urea–($x$$CeO_2$–(1 − x)MnO_2)/ACF materials were prepared. For 10% urea–($x$$CeO_2$–(1 − x)MnO_2)/ACF, the total mass percentage of the loaded oxides was 8%, in which x and 1 − x indicate the mass ratio of MnO_2 and CeO_2, respectively.

2.2. Measurement of catalytic activity

The catalytic activity of urea-SCR for NO removal was measured in a test tube 20 mm in diameter. The test tube was loaded with the sample (0.5000 g) but not packed. The experiment was carried out under the following conditions: gas velocity, 10 000 h^{-1}; NO, 1000 ppm; O_2, 21%; N_2, balanced; total flow rate, 225 mL min^{-1}; temperature, 30 °C; relative humidity, 0%. The NO concentrations were tested continuously with an NO analyzer (Auto5-1, Kane International, UK) at the inlet and outlet. The NO_2 detected at the outlet was converted to NO to obtain the final NO conversion rate. The effect of the NO concentration on the conversion of NO was investigated by using a previously reported method.[34,36] The activity of the sample was evaluated by the NO conversion rate, which was calculated by

$$\text{NO conversion}\ (\%) = \frac{NO_{x_{inlet}} - NO_{x_{outlet}}}{NO_{x_{inlet}}} \times 100\%$$

2.3. Catalytic characterization

Specific surface area, pore volume and pore diameter were determined with an ASAP 2020 analyzer. The X-ray photoelectron spectroscopy (XPS) analyses were performed at room temperature by a K-Alpha 1063 spectrometer (Thermo Fisher Scientific, UK), with an Al Kα anode (1486.6 eV) operated at 15 kV and 6 mA. The powder X-ray diffraction (XRD) patterns were obtained by using a Siemens D5000 diffractometer (German) with Cu Kα radiation in continuous scan mode from 2θ of 10° to 80° with a sampling interval of 0.02° s^{-1}. Scanning electron microscopy (SEM; 6701F, JEOL) was used to investigate the morphology of the materials. Infrared spectra were recorded on a compact Fourier transform infrared spectrophotometer (FTIR; IRAffinity-1, Shimadzu Scientific Instruments, Japan).

3. Results and discussion

3.1. Removal of NO by urea–MnO_x/ACF and urea–($x$$CeO_2$–(1 − x)MnO_2)/ACF

Fig. 1(a) shows the NO removal plane for 10% urea–MnO_x/ACF. The NO conversion ratio was strongly affected by the loading mass of MnO_x. As the mass ratio of MnO_x increased from 5% to 8%, the removal increased and reached its maximum when the loading ratio for MnO_x was 8%, suggesting that the 10% urea–MnO_x/ACF samples had the highest NO removal rate. Subsequently, the removal plane slowly decreased, indicating decreased catalytic activity. The NO removal plane for the series of 10% urea–($x$$CeO_2$–(1 − x)MnO_2)/ACF is shown in Fig. 1(b). The removal ratio of NO was 75%

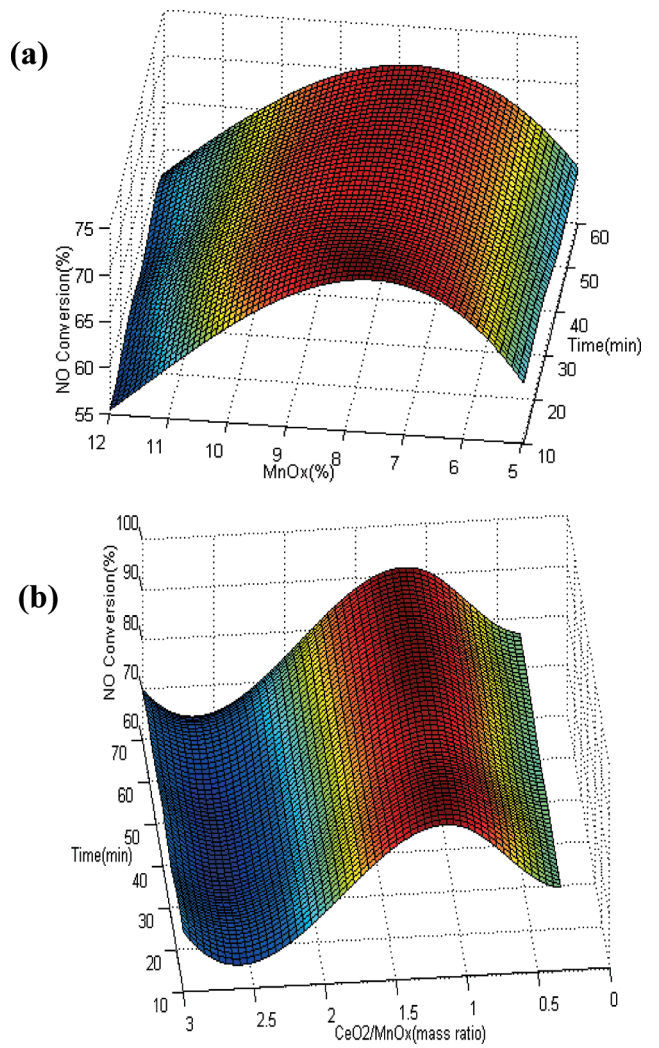

Fig. 1 SCR activity of NO. a) 10% urea–MnO_x/ACF; and b) 10% urea–($x$$CeO_2$–(1 − x)MnO_2)/ACF.

when the mass ratio of CeO_2 and MnO_x was 1 : 3, which showed its superiority compared with the samples containing MnO_x alone. As the mass ratio of CeO_2 and MnO_x changed from 1 : 3 to 1 : 1, the removal plane increased indicating that the NO conversion rate increased. When the mass ratio of CeO_2 and MnO_x was 1 : 1, the plane reached its maximum, signifying the highest NO removal of up to 90%, by 10% urea–($xCeO_2$–$(1 - x)MnO_2$)/ACF. As the mass ratio of CeO_2 and MnO_x changed from 1 : 1 to 1 : 3, the NO removal plane decreased and the NO conversion rate decreased. The results were consistent with previous research.[36] Compared with the 10% urea–(CeO_2–CuO)/ACF samples reported in our previous paper,[36] 10% urea–(0.5CeO_2–0.5MnO_2)/ACF exhibited higher NO removal when the mass ratio of the two metal oxides was 1 : 1.

3.2. Catalytic stability experiments

Fig. 2 shows the catalytic stability of 0.5000 g 10% urea–(0.5CeO_2–0.5MnO_2)/ACF for 1000 ppm NO and 21% O_2 at 30 °C. Fig. 2 shows that the NO conversion remained over 85% in the first 3 h, and then slowly decreased from 85% to 75% from 3 to 4 h. After that, the conversion rate of NO dropped quickly.

When the urea was reloaded onto 10% urea–(0.5CeO_2–0.5MnO_2)/ACF after 4 h reaction in the SCR system, its reactivity was recovered and the NO conversion ratio was scarcely affected. This demonstrated that the material could be reused after a simple, feasible treatment and its purification capacity remained almost unaffected.

3.3. Effect of NO concentration

Fig. 3 shows the performance of 10% urea–(0.5CeO_2–0.5MnO_2)/ACF in different NO concentrations (100, 200, 500, 1000 ppm).

When the concentration of NO was 100 ppm, NO conversion of over 98% could be achieved, which was much higher than for other NO concentrations. When the NO concentration increased to 500 ppm, the NO conversion rate decreased from 98% to 87%. In contrast, when the NO concentration increased from 500 to 1000 ppm, the removal of NO increased. It has been reported that the reaction of NO with urea loaded on activated carbons fiber increased as the NO concentration increased from 100 to 1000 ppm,[37] although this observation was not explained. In this paper, the effect of NO concentration on NO conversion is discussed in detail later.

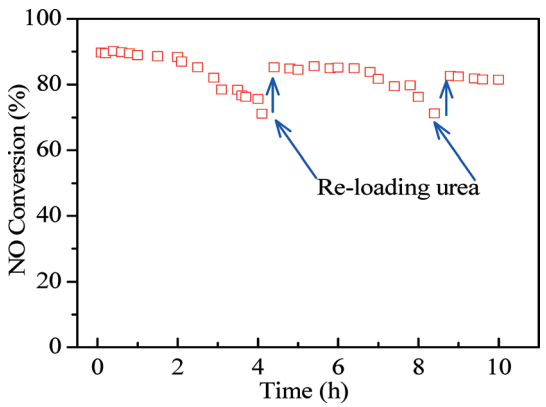

Fig. 2 Stability of 10% urea–(0.5CeO_2–0.5MnO_2)/ACF during NO removal.

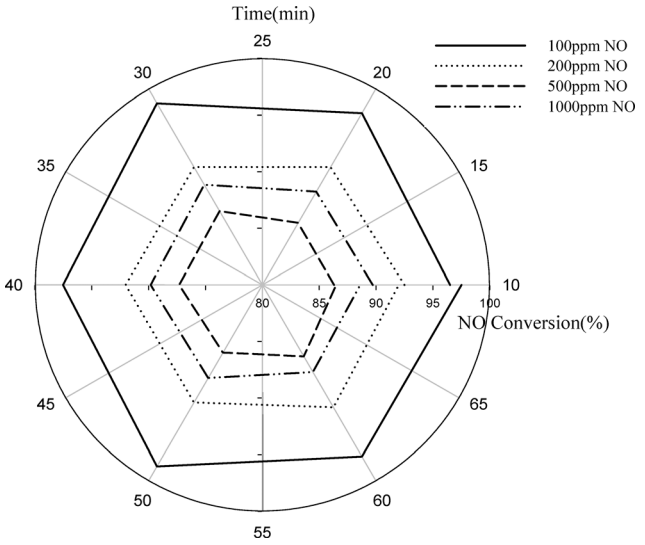

Fig. 3 Effect of NO concentration on its removal by 10% urea–(0.5CeO_2–0.5MnO_2)/ACF.

3.4. BET study

The surface areas, total pore volumes (V_t), micropore volume, and pore size of ACF, 10% urea–5% MnO_x/ACF, 10% urea–8% MnO_x/ACF, 10% urea–10% MnO_x/ACF and 10% urea–(0.5CeO_2–0.5MnO_2)/ACF are summarized in Table 1.

There was an apparent change in surface area, micropore volume (V_{micro}) and pore diameters (D_A) with the amount of urea and the mass ratios of manganese and cerium oxides loaded on ACF. As the loading of manganese oxide increased, the surface area of the sample decreased rapidly. However, the mesoporous surface area (S_{meso}) of the sample increased before decreasing. The microporous area (S_{micro}) also varied with the manganese oxide loading. This result might be explained by the dispersion of manganese and cerium oxides, which may fill the mesopores, converting some mesopores to micropores.[36,38] Meanwhile, new interconnecting pores may emerge.[38] These factors would change S_{micro}. Combined with the NO conversion rates in Fig. 1, the increase of S_{micro} and the increase in the ratio of V_{micro} to V_t may help to increase the NO conversion.[13]

3.5. XPS study

To confirm the oxidation state of the metal oxide loaded on ACF and to understand the catalytic mechanism in the NO conversion process, 10% urea–8% MnO_x/ACF and 10% urea–(0.5CeO_2–0.5MnO_2)/ACF were characterized by XPS.

Table 1 Surface area, pore volume and pore size of the catalysts

Sample	S_{BET} (m^2 g^{-1})	S_{meso} (m^2 g^{-1})	S_{micro} (m^2 g^{-1})	V_t (cm^3 g^{-1})	V_{micro} (cm^3 g^{-1})	D_A (nm)
ACF	1491.23	751.72	739.51	0.71	0.34	19.16
10% urea–5% MnO_x/ACF	1447.39	769.66	677.73	0.69	0.31	19.20
10% urea–8% MnO_x/ACF	1386.59	642.86	743.73	0.66	0.34	19.21
10% urea–10% MnO_x/ACF	1339.34	624.28	715.06	0.64	0.33	19.21
10% urea–($0.5CeO_2$–$0.5MnO_2$)/ACF	1234.42	605.76	628.66	0.60	0.29	19.36

Table 2 shows the surface atomic concentrations of Mn, Ce, O and N. The atomic ratio of manganese and cerium on the surface of ACF was less than 1 : 1. This may indicate that cerium oxides were dispersed on the surface of ACF, whereas the manganese oxides were embedded in the mesopores of ACF.[36]

Fig. 4(a) shows the Mn 2p binding energy peaks in 10% urea–8% MnO_x/ACF, which suggested the coexistence of Mn^{4+} and Mn^{3+}. Fig. 3(a) shows that Mn^{3+} had 2p 3/2 and 2p 1/2 peaks with binding energies of 641.3 and 653.2 eV, whereas the binding energies of Mn^{4+} for 2p 3/2 and 2p 1/2 were 642.9 and 654.5 eV, respectively.[39,40]

The existence of various manganese valences may increase the electron transfer during the NO conversion processes.[39] *Via* the reduction of Mn^{4+} to Mn^{3+}, the lattice oxygen was released. The additional lattice oxygen generated in the catalytic system, which was more reactive than the oxygen adsorbed from the mixed gas, increased the conversion of NO to NO_2 greatly at room temperature.[36] This was consistent with the experimental results illustrated in Fig. 1.

Fig. 4(b) and (c) show the Mn 2p and Ce 3d binding energy peaks for 10% urea–($0.5CeO_2$–$0.5MnO_2$)/ACF, respectively. Mn^{3+} (641.1 and 652.6 eV), Mn^{4+} (642.6 and 654.0 eV), Ce^{3+} (886.1 and 904.5 eV) and Ce^{4+} (882.3 and 900.3 eV)[41,42] were detected on the surface of the sample. Because electron transfer from Ce^{3+} to Ce^{4+} was much easier than that from Mn^{3+} to Mn^{4+},[23] more lattice oxygen was released *via* the interaction between the redox couple of Ce^{4+}/Ce^{3+} and Mn^{4+}/Mn^{3+}. Therefore, NO conversion to NO_2 with 10% urea–$Ce_xMn_{1-x}O_2$/ACF was much easier than that with 10% urea–MnO_x/ACF, which resulted in higher NO conversion. This was consistent with the experimental results in Fig. 1.

Fig. 5(a) and (b) show the XPS O 1s spectra of 10% urea–8% MnO_x/ACF and 10% urea–($0.5CeO_2$–$0.5MnO_2$)/ACF, respectively. Fig. 5(a) shows that the peak at 530.0 eV arose from the lattice oxygen of manganese oxide,[42,43] the BE peak at 531.4 eV was from the hydroxyl groups,[44] and the BE peak at 532.3 eV was attributed to the oxygen in the C═O bond of urea.[44,45] In Fig. 5(b), the binding energy peak of the lattice oxygen in the metal oxide was at 530.7 eV. The peaks at 531.4 and 532.8 eV corresponded to the oxygen of the hydroxyl groups and the oxygen in the C═O bond of urea, respectively. Fig. 5(a) and (b) show that the binding energy of the lattice oxygen and the oxygen in the C═O bond of urea in 10% urea–($0.5CeO_2$–$0.5MnO_2$)/ACF was slightly higher than that in 10% urea–MnO_x/ACF. Therefore, the binding energy of O 1s in CeO_2 was higher than in MnO_x and the difference in the O 1s binding energy of the lattice oxygen and the oxygen in the C═O bond of urea in the two samples suggests that there may be an interaction between urea and the metal oxide.

Table 2 Atomic percentage of elements detected on the surface of the catalysts

	Element			
Sample	Mn 2p	Ce 3d	O 1s	N 1s
10% urea–8% MnO_x/ACF	20.5	—	55.8	13.5
10% urea–($0.5CeO_2$–$0.5MnO_2$)/ACF	4.3	9.3	45.3	33.4

3.6. XRD study

The XRD patterns of 10% urea–($0.5CeO_2$–$0.5MnO_2$)/ACF are shown in Fig. 6. The XRD patterns contained graphite-like crystallites at 20–30° and 40–50°.[13,46] However, there were no sharp, clear peaks for the metal oxides. This may be because the mass ratio of the metal oxides loaded on ACF of about 8% was low and the metal oxides were not well crystallized on the surface of ACF. The SEM image of the sample showed that the metal oxides were well dispersed on ACF, which may also have led to the weak peaks in the XRD pattern.

After 10% urea–($0.5CeO_2$–$0.5MnO_2$)/ACF underwent the SCR with NO for 4 h, the XRD pattern was almost unchanged, demonstrating that the graphite-like crystallites changed little owing to the involvement of NO in the SCR.[23,47] 10% urea–($0.5CeO_2$–$0.5MnO_2$)/ACF could be reused after the urea was reloaded, which was consistent with the results in Fig. 2.

3.7. FTIR study

To understand the physical properties of the samples, which could affect the catalytic activity of the material strongly, FTIR experiments were conducted. The results are shown in Fig. 7.

Fig. 7(a) shows that the chemical groups of different 10% urea–MnO_x/ACF materials displayed considerable differences as the mass ratio of manganese oxide loaded on the 10% urea/ACF increased. The modification with the metal oxide changed the wavenumber bands and half-peak height. The main bands of 10% urea/ACF were at 3440, 1640, and 2360 cm^{-1} and weak bands were between 1400 and 1600 cm^{-1}. The bands for 10% urea–MnO_x/ACF were primarily at 3440, 2360, 1100, and 670 cm^{-1}. In Fig. 7 (b), the main bands of 10% urea–$0.5CeO_2$–$0.5MnO_2$/ACF were at 3440 and 2360 cm^{-1}, and the weak bands were between 1100 and 500 cm^{-1}.

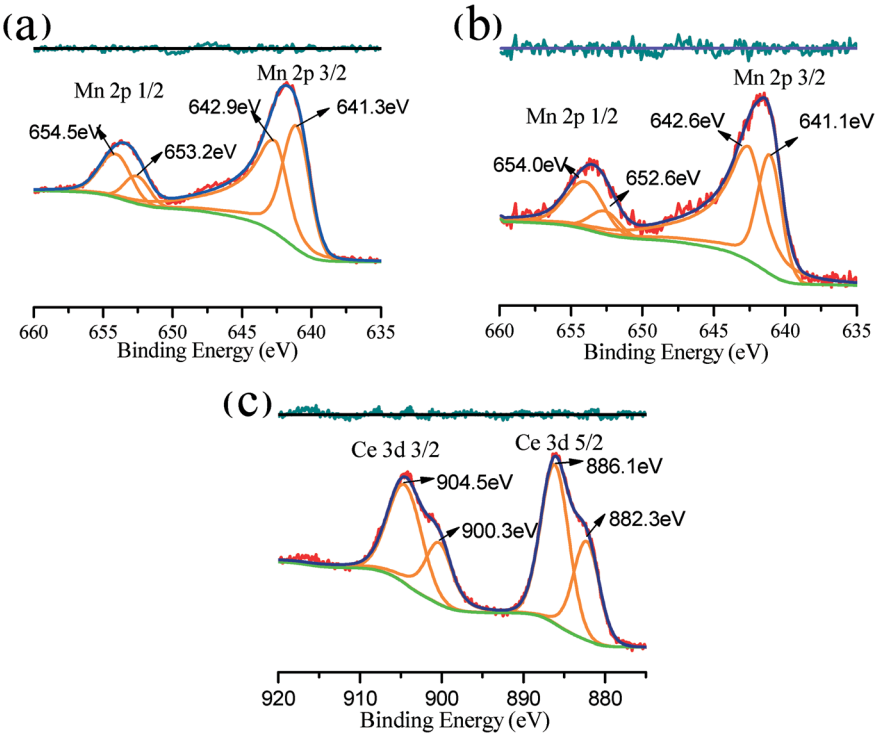

Fig. 4 XPS results. a) Mn 2p 1/2 and 2p 3/2 spectrum for 10% urea–8% MnO_x/ACF; b) Mn 2p 1/2 and 2p 3/2 spectrum for 10% urea–(0.5CeO_2–0.5MnO_2)/ACF; and c) Ce 3d 3/2 and 3d 5/2 spectrum for 10% urea–(0.5CeO_2–0.5MnO_2)/ACF.

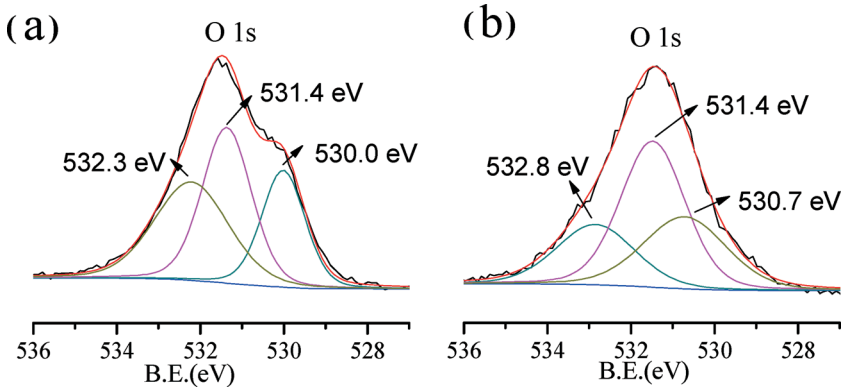

Fig. 5 O 1s XPS spectra. a) 10% urea–8% MnO_x/ACF; and b) 10% urea–(0.5CeO_2–0.5MnO_2)/ACF.

The band at 3440 cm^{-1} was the hydroxyl group,[13,25,35] which was consistent with the binding energy peak of 531.4 eV in the XPS O 1s spectra. The weak bands between 1400 and 1640 cm^{-1} were ascribed to the adsorption of NO_2 gas generated during pyrolysis adsorbed on the ACF, and corresponded to the vibration of bidentate nitrate or monodentate nitrite.[13,25] Comparing the FTIR spectra of different samples suggested that the band at 2360 cm^{-1} may arise from the interaction between urea and the metal oxide.[24,25] The band at 2360 cm^{-1} was weak when only urea was loaded on ACF. The band at 2360 cm^{-1} appeared when the metal oxide and urea were both loaded on ACF. However, when the urea loaded on the catalyst was exhausted after the SCR, the band became weak again. This was consistent with the discussion of the XPS O 1s spectra above. The band at 2360 cm^{-1} might be beneficial to the catalytic process for manganese oxide loaded on urea-ACF.

3.8. Mechanism discussion

Next, we discuss the catalytic mechanism for the selective catalytic reduction of NO with urea–MnO_x/ACF. Because the oxidation of NO to NO_2 is the key step in the reduction of NO with urea on carbon materials,[34,37] the reduction of NO with urea would be greatly improved if the oxidation of NO could be promoted catalytically. Because the XPS spectra of 10%

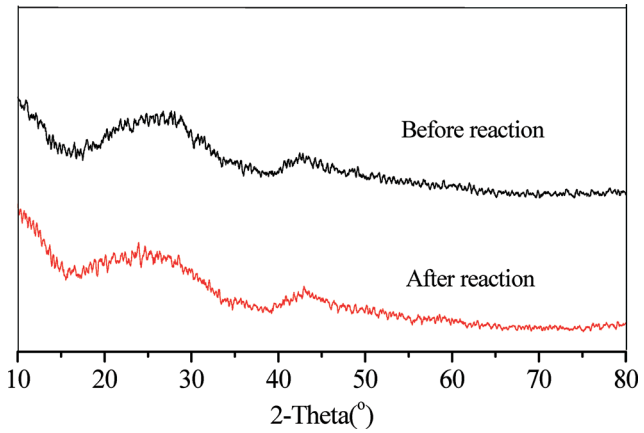

Fig. 6 XRD spectrum of 10% urea–(0.5CeO_2–0.5MnO_2)/ACF.

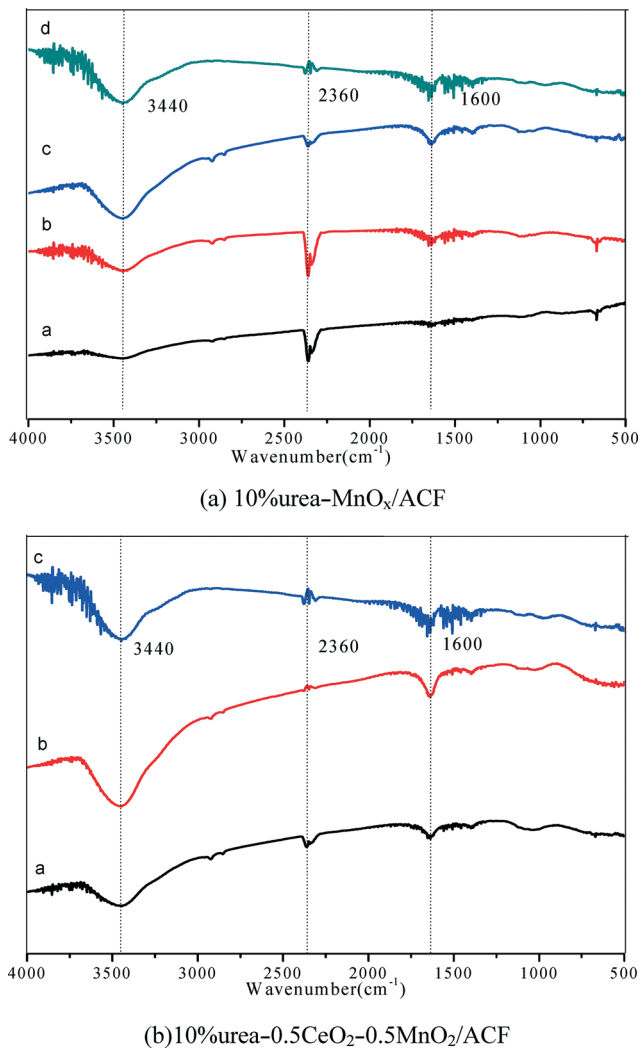

Fig. 7 FTIR spectra of the catalysts. a) 10% urea–MnO_x/ACF; and b) 10% urea–(0.5CeO_2–0.5MnO_2)/ACF.

urea–8% MnO_x/ACF indicated that Mn^{4+} and Mn^{3+} co-existed on the surface, it could be concluded that the reaction of MnO_2 during the catalysis might occur as shown in eqn (1). The additional lattice oxygen produced in reaction promoted the oxidation of NO to NO_2 (eqn (3)).[23]

$$2MnO_2 \leftrightarrows Mn_2O_3 + O^{\bullet} \quad (1)$$

$$2CeO_2 \leftrightarrows Ce_2O_3 + O^{\bullet} \quad (2)$$

$$NO + O^{\bullet} \rightarrow NO_2 \quad (3)$$

In the XPS spectrum of 10% urea–(0.5CeO_2–0.5MnO_2)/ACF, Ce^{4+} and Ce^{3+} were detected as well as Mn^{4+} and Mn^{3+}. Based on the interaction between MnO_2 and Mn_2O_3 and between CeO_2 and Ce_2O_3 shown in eqn (2), a synergetic effect[23,48] between manganese and cerium was expected to contribute to the catalytic process. The interplay between cerium and manganese in the catalytic process followed the reactions in eqn (4)–(7).

$$Mn_{(ads)}^{4+} + NO \leftrightarrows Mn_{(ads)}^{3+} + NO_{(ads)}^{+} \quad (4)$$

$$Mn_{(ads)}^{3+} + Ce_{(ads)}^{4+} \leftrightarrows Mn_{(ads)}^{4+} + Ce_{(ads)}^{3+} \quad (5)$$

$$Ce_{(ads)}^{3+} + 1/2O_2 \leftrightarrows Ce_{(ads)}^{4+} + O_{(ads)}^{-} \quad (6)$$

$$NO_{(ads)}^{+} + O_{(ads)}^{-} \rightarrow NO_2 \quad (7)$$

Because urea was loaded on the samples, the interaction between urea and the metal oxides played an important role in the system. The reaction on the surface of ACF involved eqn (4)–(10). Initially, the active sites of the metal oxides were mainly occupied by urea, and most NO was reduced to N_2 directly by the urea at the active sites on the surface of ACF according to eqn (8) when the NO concentration was low. As the concentration of NO increased, the active sites of the metal oxide began to be dominated by NO. Through the reactions in eqn (4)–(7), NO was converted to NO_2, which reacts easily with urea on ACF.[33]

There was competition for the active sites between urea and NO, which our experimental results showed impeded the reduction of NO. Although the reaction of urea with NO in the active sites and the reaction of NO_2 with urea that was not in the active sites both promoted the reduction of NO, the difference between the two reactions was great, and the reactions may compete. The reaction of urea in the active sites with NO may limit the reaction of NO_2 with urea that is not in the active site, decreasing the amount of NO being oxidized to NO_2. Because NO is small, it occupies the active sites of the metal oxides loaded with urea more efficiently.

However, when the concentration of NO was low, the advantage of size was small and the NO conversion rate decreased with the decrease in the number of active sites occupied by urea. When the NO concentration increased to 500 ppm, the two reactions were equivalent and the NO conversion rate reached a minimum. When the NO concentration increased above 500 ppm, the active sites were mainly occupied by NO, and the reaction of NO_2 with urea that was

not in the active site became dominant. Therefore, the NO conversion rate increased. The mechanism in this study with NO at low and high concentrations was similar to the Eley–Rideal mechanism and Langmuir–Hinshelwood mechanism in NH_3 SCR, respectively.[1,23,24] However, the urea reducing agent was pre-loaded on the surface and did not need to be adsorbed from the mixed gases, and thus initially urea had the advantage over NO in occupying the active sites.

In the urea/ACF system, there was no such competition between urea and NO. The catalytic oxidation of NO to NO_2 was mainly achieved by ACF and it increased greatly as NO concentration increased. The higher the NO concentration, the higher the NO conversion to NO_2,[49] and higher NO reduction to N_2 was achieved after the reaction in eqn (8) together with the reactions in eqn (9) and (10).

$$4NO + O_2 + 2(NH_2)_2CO \rightarrow 4N_2 + 2CO_2 + 4H_2O \quad \Delta G_1 = -1798.28 \text{ kJ mol}^{-1} \tag{8}$$

$$2NO_2 + 2(NH_2)_2CO + O_2 \rightarrow 3N_2 + 2CO_2 + 4H_2O \quad \Delta G_2 = -1410.64 \text{ kJ mol}^{-1} \tag{9}$$

$$NO + NO_2 + (NH_2)_2CO \rightarrow 2N_2 + CO_2 + 2H_2O \quad \Delta G_3 = -791.89 \text{ kJ mol}^{-1} \tag{10}$$

3.9. Kinetic discussion

The pseudo-first order rate constant (k) can be calculated by[11,12,33]

$$k = -\frac{F}{W}\ln(1-S) \tag{11}$$

where F is the total rate (mL s^{-1}), W is the mass of the catalyst (g) and S is the ratio of NO conversion.

The adsorption of the urea on the catalyst follows eqn (12)–(16)[11,12]

$$(NH_2)_2CO \leftrightarrows (NH_2)_2CO^* \tag{12}$$

$$(NH_2)_2CO^* + \equiv M^{4+} \rightarrow -NH_2 + \equiv M^{3+} + NH_2CO^+ \tag{13}$$

$$NH_2CO^+ + \equiv M^{4+} + O^{2-} \rightarrow -NH_2 + \equiv M^{3+} + CO_2 \tag{14}$$

$$-NH_2 + NO_{(g)} \rightarrow N_2 + H_2O \tag{15}$$

$$\equiv M^{3+} + 1/4O_2 \rightarrow \equiv M^{4+} + 1/2\equiv O^{2-} \tag{16}$$

where * indicates the species adsorbed on the surface of the catalyst and M represents manganese and cerium.

The kinetic equation of eqn (15) can be written as

$$-\frac{d[-NH_2]}{dt} = -\frac{d[NO_{(g)}]}{dt} = \frac{d[N_2]}{dt} = k_1[-NH_2][NO_{(g)}] \tag{17}$$

where k_1 is the kinetic constant of reaction (15).

In eqn (13) and (14), when the surface of catalyst is saturated with the adsorption of $-NH_2$, $[-NH_2]$ is a constant which can be approximated as

$$[-NH_2] = [M^{4+}]\{k_2[(NH_2)_2CO^*] + k_3[NH_2CO^+]\} \tag{18}$$

where k_2 and k_3 are constants in the equation, and the concentration of reducible M^{4+}, $[M^{4+}]$, is the kinetic constant.

Therefore, based on the kinetic equation above, we obtain the equations

$$\int \frac{d[NO_{(g)}]}{NO_{(g)}} = -\int k_1\left\{k_2[(NH_2)_2CO^*] + k_3[NH_2CO^+]\right\}[M^{4+}]dt \tag{19}$$

$$\int_{[NO_{(g)}]_{in}}^{[NO_{(g)}]_{t'}} \frac{d[NO_{(g)}]}{[NO_{(g)}]} = -\int_0^{t'} k_1\left\{k_2[(NH_2)_2CO^*] + k_3[NH_2CO^+]\right\}[M^{4+}]dt \tag{20}$$

where $[NO_{(g)}]_{in}$ is the initial NO concentration. Therefore, the gaseous NO concentration in the specific part of the catalyst column ($[NO_{(g)}]_{t'}$) can be written

$$[NO_{(g)}]_{t'} = [NO_{(g)}]_{in}\exp(-k_1\{k_2[(NH_2)_2CO^*] + k_3[NH_2CO^+]\}[M^{4+}]t') \tag{21}$$

where t' is the time it took for NO to reach the specific part of catalyst column. The whole kinetic equation can be written as

$$\begin{aligned} -\frac{d[NO_{(g)}]}{dt} &= \int_0^{t^*} d[NO_{(g)}]_{t'} = \int_0^{t^*} k_1\left\{k_2[(NH_2)_2CO^*] + k_3[NH_2CO^+]\right\}[M^{4+}][NO_{(g)}]_{t'}dt' \\ &= k_1\left\{k_2[(NH_2)_2CO^*] + k_3[NH_2CO^+]\right\}[M^{4+}][NO_{(g)}]_{in} \\ &\times \int_0^{t^*} k_1\left\{k_2[(NH_2)_2CO^*] + k_3[NH_2CO^+]\right\}[M^{4+}]t')dt' \end{aligned} \tag{22}$$

where t^* is a constant equal to the reciprocal of GHSV.

As the NO concentration increases, the chain reaction below becomes dominant.

$$(NH_2)_2CO \leftrightarrows (NH_2)_2CO^* \tag{12}$$

$$NO_{(g)} \leftrightarrows NO^* \tag{23}$$

$$NO^* + \equiv M^{4+} + O^{2-} \rightarrow NO_2^- + \equiv M^{3+} \tag{24}$$

$$NO_2^- + (NH_2)_2CO^* \rightarrow N_2 + 2OH^- + NH_2CO^+ \tag{25}$$

$$NO_2^- + NH_2CO^+ \rightarrow N_2 + H_2O + CO_2 \quad (26)$$

$$\equiv M^{3+} + 1/4O_2 \rightarrow \equiv M^{4+} + 1/2\equiv O^{2-} \quad (27)$$

The concentration of NO in the mixture was high enough to reach the saturation of its adsorption on the surface, particularly in the supported system, in which ACF could serve as a reservoir for NO. Therefore, the concentration of NO*, [NO*], was constant. The reaction of NO_2^- with $(NH_2)_2CO^*$ and NH_2CO^+ in the reactions in eqn (25) and (26) are equivalent to the reaction of NO_2^- with NH_2^*. Thus, eqn (25) and (26) can be written

$$NO_2^- + - NH_2^* \rightarrow N_2 + 2OH^- \quad (28)$$

The concentration of $-NH_2^*[-NH_2^*]$ is proportional to $[(NH_2)_2CO^*]$ and $[NH_2CO^+]$ as

$$[-NH_2^*] = k_4\{k_5[(NH_2)_2CO^*] + k_6[NH_2CO^+]\} \quad (29)$$

where k_4, k_5, and k_6 are constants.

The kinetic equations for reactions (24) and (28) can be written

$$-\frac{d[NO^*]}{dt} = -\frac{d[M^{4+}]}{dt} = \frac{d[NO_2^-]}{dt} = k_7[NO^*][M^{4+}] \quad (30)$$

$$-\frac{d[NO_2^-]}{dt} = -\frac{d[-NH_2^*]}{dt} = \frac{d[N_2]}{dt} = k_8[NO_2^-][-NH_2^*] \quad (31)$$

where k_7 and k_8 are the kinetic constants for eqn (24) and (28), respectively. $[NO_2^-]$ is the concentration of NO_2^- and $[M^{4+}]$ is the concentration of reducible M^{4+}, both of which are kinetic constants. When the chemical adsorption of NO_2^- is saturated on the surface, $[NO_2^-]$ is constant.

$$[NO_2^-] = \int_0^t k_7[NO^*][M^{4+}]dt = k_9[NO^*][M^{4+}] \quad (32)$$

Here, k_9 is a constant in the equation, which relates to the oxidation of NO* in eqn (24). Then, eqn (31) can be written

$$-\frac{d[NO_2^-]}{dt} = -\frac{d[-NH_2^*]}{dt} = \frac{d[N_2]}{dt} = k_4k_8k_9[NO^*][M^{4+}]\{k_5[(NH_2)_2CO^*] + k_6[NH_2CO^+]\} \quad (33)$$

Hence, the catalytic reduction of NO can be integrated as

$$-\frac{d[NO_{(g)}]}{dt} = k_4k_8k_9[NO^*][M^{4+}]\{k_5[(NH_2)_2CO^*] + k_6[NH_2CO^+]\}t^* \quad (34)$$

where t^* is the reciprocal of GHSV.

Therefore, the kinetic discussion indicates that the catalytic efficiency of NO was greatly affected by the BET surface area of the samples and the catalytic reactivity of the transition metal oxide. A high BET area and catalytic activity generated a large amount of NO* or $(NH_2)_2CO^*$ that rapidly reacted with NO, which resulted in the significant increase in NO conversion. This mechanism is consistent with the experimental results.

4. Conclusions

In this study, a reusable material with high NO removal performance was prepared. ACF loaded with urea and Mn–Ce mixed oxides achieved high NO conversion at room temperature. Urea–($0.5CeO_2$–$0.5MnO_2$)/ACF showed the highest catalytic activity of the materials owing to its superior synergetic effect between manganese and cerium. Moreover, the NO concentration affected the NO conversion strongly. When the NO concentration was 100 ppm, NO conversion of over 98% was achieved by urea–($0.5CeO_2$–$0.5MnO_2$)/ACF. In particular, 10% urea–($0.5CeO_2$–$0.5MnO_2$)/ACF was regenerated by reloading with urea. Therefore, the material developed in this work is efficient enough to remove NO from the atmosphere at room temperature at NO concentrations below 100 ppm.

Acknowledgements

This work was supported by the Joint Funds of the National Natural Science Foundation of China (Grant No. U1560110), the National Natural Science Foundation of China (Grant No. 51108169) and Fundamental Research Funds for the Central Universities.

References

1 G. S. Qi and R. T. Yang, *J. Catal.*, 2003, **217**, 434.
2 C. E. Stere, W. Adress, R. Burch, S. Chansai, A. Goguet, W. G. Graham, F. De Rosa, V. Palma and C. Hardacre, *ACS Catal.*, 2014, **4**, 666.
3 D. L. TorreUnai, P.-A. Beñat and G.-V. R. Juan, *Chem. Eng. J.*, 2012, **207–208**, 10.
4 X. Wang, W. Wen, J. Mi, X. Li and R. Wang, *Appl. Catal., B*, 2015, **176–177**, 454.
5 C. N. Costa and A. M. Efstathiou, *Appl. Catal., B*, 2007, **72**, 240.
6 J. H. Li, Y. Q. Zhu, R. Ke and J. M. Hao, *Appl. Catal., B*, 2008, **80**, 202.
7 P. Sazama, L. Čapek, H. Drobná, Z. Sobalík, J. Dědeček, K. Arve and B. Wichterlová, *J. Catal.*, 2005, **232**, 302.
8 Y. J. Kim, J. K. Lee, K. M. Min, S. B. Hong, I.-S. Nam and B. K. Cho, *J. Catal.*, 2014, **311**, 447.
9 T. Boningari, P. R. Ettireddy, A. Somogyvari, Y. Liu, A. Vorontsov, C. A. McDonald and P. G. Smirniotis, *J. Catal.*, 2015, **325**, 145.
10 M. Yasuda, N. Tsugita, K. Ito, S. Yamauchi, W. R. Glomm, I. Tsuji and H. Asano, *Environ. Sci. Technol.*, 2011, **45**, 1840.
11 S. J. Yang, C. Z. Wang, J. H. Li, N. Q. Yan, L. Ma and H. Z. Chang, *Appl. Catal., B*, 2011, **110**, 71.

12 S. J. Yang, J. H. Li, C. Z. Wang, J. H. Chen, L. Ma, H. Z. Chang, L. Chen, Y. Peng and N. Q. Yan, *Appl. Catal., B*, 2012, **117–118**, 73.
13 P. Lu, C. T. Li, G. M. Zeng, L. J. He, D. L. Peng, H. F. Cui, S. H. Li and Y. B. Zhai, *Appl. Catal., B*, 2010, **96**, 157.
14 C. T. Li, P. Lu, G. M. Zeng, Q. J. Wang, Q. Li, L. J. He and Y. B. Zhai, *Huanjing Kexue*, 2008, **29**, 3280.
15 L. Gutierrez and E. A. Lombardo, *Appl. Catal., A*, 2009, **360**, 107.
16 P. S. Metkar, N. Salazar, R. Muncrief, V. Balakotaiah and M. P. Harold, *Appl. Catal., B*, 2011, **104**, 110.
17 P. Sazama, B. Wichterlová, E. Tábor, P. Šťastný, N. K. Sathu, Z. Sobalík, J. Dědeček, Š. Sklenák, P. Klein and A. Vondrová, *J. Catal.*, 2014, **312**, 123.
18 Z. Zeng, P. Lu, C. T. G. M. Zeng and X. Jiang, *J. Coord. Chem.*, 2012, **65**, 1992.
19 J. H. Huang, Z. Q. Tong, Y. Huang and J. F. Zhang, *Appl. Catal., B*, 2008, **78**, 309.
20 Y. S. Shen, S. M. Zhu, T. Qiu and S. B. Shen, *Catal. Commun.*, 2009, **11**, 20.
21 H. Li, X. L. Tang, H. H. Yi and L. L. Yu, *J. Rare Earths*, 2010, **28**, 64.
22 K. Tikhomirov, O. Krocher, M. Elsener and A. Wokaun, *Appl. Catal., B*, 2006, **64**, 72.
23 G. S. Qi, R. T. Yang and R. Chang, *Appl. Catal., B*, 2004, **51**, 93.
24 G. S. Qi and R. T. Yang, *J. Phys. Chem. B*, 2004, **108**, 15738.
25 B. X. Shen, H. Q. Ma and Y. Yao, *J. Environ. Sci.*, 2012, **24**, 499.
26 U. Diebold, *Surf. Sci. Rep.*, 2003, **48**, 53.
27 J. Miyawaki, T. Shimohama, N. Shimohama, A. Yasutake, M. Yoshikawa, I. Mocjida and S.-H. Yoon, *Appl. Catal., B*, 2011, **110**, 273.
28 A. Trapalis, N. Todorova, T. Giannakopoulou, N. Boukos, T. Speliotis, D. Dimotikali and J. Yu, *Appl. Catal., B*, 2016, **180**, 637.
29 Q. Yu, H. Wang, T. Liu, L. Xiao, X. Jiang and X. Zheng, *Environ. Sci. Technol.*, 2012, **46**, 2337.
30 Z. Zeng, P. Lu, C. T. Li, L. Mai, Z. Li and Y. S. Zhang, *Catal. Sci. Technol.*, 2012, **2**, 2188.
31 J. S. Moon, K. K. Park, J. H. Kim and G. Seo, *Appl. Catal., A*, 1999, **184**, 41.
32 M. Koebel, M. Elsener and M. Kleemann, *Catal. Today*, 2000, **59**, 335.
33 N. Shirahama, I. Mochida, Y. Korai, K. H. Choi, T. Enjoji, T. Shimohara and A. Yasutake, *Appl. Catal., B*, 2004, **52**, 173.
34 P. Lu, Z. Zeng, C. T. Li, G. M. Zeng, J. Guo, X. Jiang, Y. B. Zhai and X. P. Fan, *Environ. Technol.*, 2012, **33**, 1029.
35 Z. Zeng, P. Lu, C. T. Li, G. M. Zeng, X. Jiang, Y. B. Zhai and X. P. Fan, *Environ. Technol.*, 2012, **33**, 1331.
36 X. Jiang, P. Lu, C. T. Li, Z. Zeng, G. M. Zeng, L. P. Hu, L. Mai and Z. Li, *Environ. Technol.*, 2013, **34**(5), 591–598.
37 N. Shirahama, I. Mochida, Y. Korai, K. H. Choi, T. Enjoji, T. Shimohara and A. Yasutake, *Appl. Catal., B*, 2005, **57**, 237.
38 M. Molina-Sabio, M. T. Gonzalez, F. Rodriguez-Reinoso and A. Sepúlveda-Escribano, *Carbon*, 1996, **34**, 505.
39 S. M. Lee, K. H. Park and S. C. Hong, *Chem. Eng. J.*, 2012, **195–196**, 323.
40 W. J. Hong, S. Iwamoto, S. Hosokawa, K. Wada, H. Kanai and M. Inoue, *J. Catal.*, 2011, **277**, 208.
41 P. Li, P. Lu, Y. Zhai, C. Li, T. Chen, R. Qing and W. Zhang, *Environ. Technol.*, 2015, **18**, 2390.
42 L. Shi, W. Chu, F. Qu and S. Luo, *Catal. Lett.*, 2007, **113**, 59.
43 M. Machida, M. Uto and D. Kurogi, *Chem. Mater.*, 2000, **12**, 3158.
44 M. Alifanti, B. Baps, N. Blangenois, J. Naud, P. Grange and B. Delmon, *Chem. Mater.*, 2003, **15**, 395.
45 J. F. Moulder, W. F. Sticle, P. E. Sobol and K. D. Bomben, *Handbook of XPS*, ed. J. Chastain, Perkin-Elmer Corporation, Wellesley, MA, 1992.
46 L. L. Zhu, B. C. Huang, W. H. Wang, Z. L. Wei and D. Q. Ye, *Catal. Commun.*, 2011, **12**, 394.
47 M. A. Daley, D. Tandon, J. Economy and E. J. Hippo, *Carbon*, 1996, **34**, 1191.
48 G. Carja, Y. Kameshima, K. Okada and C. D. Madhusoodana, *Appl. Catal., B*, 2007, **73**, 60.
49 S. Adapa, V. Gaur and N. Verma, *Chem. Eng. J.*, 2006, **116**, 25.

